International Journal of Non-Linear Mechanics 44 (2009) 200–208

Contents lists available at ScienceDirect

International Journal of Non-Linear Mechanics

journal homepage: www.elsevier.com/locate/nlm

Buckling and post-buckling of extensible rods revisited: A multiple-scale solution

Carlos E.N. Mazzilli*

Department of Structural and Geotechnical Engineering, Escola Politécnica, University of São Paulo, Av. Prof. Almeida Prado, trav.2 n. 83, São Paulo 05508-900, Brazil

ARTICLE INFO

Article history:
Received 14 April 2008
Received in revised form 29 September 2008
Accepted 12 November 2008

Keywords:
Buckling
Extensible rod
Elastic instability
Post-buckling
Method of multiple scales

ABSTRACT

An exact non-linear formulation of the equilibrium of elastic prismatic rods subjected to compression and planar bending is presented, electing as primary displacement variable the cross-section rotations and taking into account the axis extensibility. Such a formulation proves to be sufficiently general to encompass any boundary condition. The evaluation of critical loads for the five classical Euler buckling cases is pursued, allowing for the assessment of the axis extensibility effect. From the quantitative viewpoint, it is seen that such an influence is negligible for very slender bars, but it dramatically increases as the slenderness ratio decreases. From the qualitative viewpoint, its effect is that there are not infinite critical loads, as foreseen by the classical inextensible theory. The method of multiple (spatial) scales is used to survey the post-buckling regime for the five classical Euler buckling cases, with remarkable success, since very small deviations were observed with respect to results obtained via numerical integration of the exact equation of equilibrium, even when loads much higher than the critical ones were considered. Although known beforehand that such classical Euler buckling cases are imperfection insensitive, the effect of load offsets were also looked at, thus showing that the formulation is sufficiently general to accommodate this sort of analysis.

1. Introduction

This paper should not begin without recalling the magisterial work by Euler [1] published 268 years ago, in which variational methods were applied to determine the "elastica" and buckling loads of inextensible rods, based on kinematical hypothesis suggested by Bernoulli [2]. Since then, the subject has been extensively studied, as seen in [3–8], due to its utmost relevance to the design of reticulated structures.

Also, this paper recasts and expands works written by the author more than 20 years ago [9,10]. The general non-linear equation of equilibrium of 2D Bernoulli–Euler elastic beam-columns subjected to end bending moment and compression force with possible loading offset (imperfection) is written in terms of cross-section rotations, taking into account axial stretching.

The general linearised equation is examined in order to evaluate critical loads for each one of the five classic Euler buckling cases, considering different constraint conditions [3,4]. Such critical loads are compared to the classical values for inextensible bars and conclusions are drawn with regard to the number of critical loads.

Next, the non-linear equation of equilibrium is recast and the post-buckling regime is surveyed using the method of multiple scales to produce a single explicit solution that is valid for any one of the five classic cases. Unlike the basic perturbation techniques used in non-linear statics, such as the straightforward expansion method (Poincaré's method) [11], which are barely capable of estimating the initial post-buckling response, the method of multiple scales [12] is able to supply a very accurate estimate of the displacements for loads much higher than the critical one, as seen when a comparison is made with results of numerical integration. The method of multiple scales is known for rendering uniformly convergent expansions, which is a most valuable feature in non-linear dynamics, where the independent variable (time) ranges from zero to infinity. In non-linear statics, the variation of the independent variable (co-ordinate along the bar axis) is comfortably limited to the bar length. It was already surprising to the author 20 years ago and so it is even more now, that very little attention has been given to the remarkable power of the multiple scales expansions to supply at the same time simple and accurate results in non-linear statics. In fact, only a few references on the use of the method of multiple scales in non-linear statics can be reported in the literature, as in [13,14].

Although the classical elastic Euler buckling cases are known to be imperfection insensitive [6,7], both the perfect and imperfect responses are inter-compared for the clamped-free and the hinged–hinged rods, as illustrative examples of the formulation generality.

* Tel.: +55 1130915232.
E-mail address: cenmazzi@usp.br

0020-7462/$ - see front matter © 2008 Elsevier Ltd. All rights reserved.
doi:10.1016/j.ijnonlinmec.2008.11.005

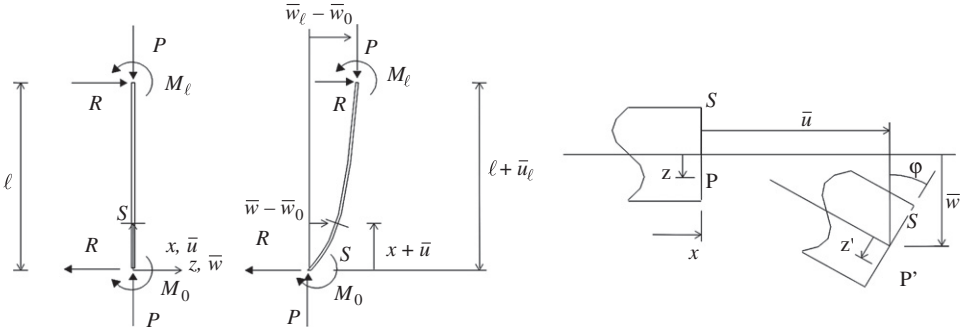

Fig. 1. (a) Prismatic elastic rod under bending and compression; (b) Bernoulli–Euler beam kinematics.

2. Non-linear equilibrium equation

The prismatic beam-column of Fig. 1(a), with length ℓ, cross-section area A and moment of inertia I, made of an elastic material of Young's modulus E, is considered. It is subjected to an initial axial compression P. It may be the case that end-bending moments come into play, as result of constraint conditions and/or load offsets. In the general case, to restore equilibrium with respect to moments, it may happen that end transversal forces R also appear.

Fig. 1(b) introduces the notation and refers to the Bernoulli–Euler kinematics, which is characterised by the following well-known relationships:

$$u = \bar{u} - z\sin\varphi,$$

$$w = \bar{w} - z(1-\cos\varphi),$$

$$\sin\varphi = \frac{\bar{w}'}{\bar{\lambda}} \;\Rightarrow\; \bar{w}' = \bar{\lambda}\sin\varphi,$$

$$\cos\varphi = \frac{1+\bar{u}'}{\bar{\lambda}} \;\Rightarrow\; 1+\bar{u}' = \bar{\lambda}\cos\varphi, \tag{1}$$

where u and w stand for the axial and transversal displacements of a point P that in the undeformed configuration is given by (x,z); $\bar{u}$ and $\bar{w}$ are the corresponding displacements for the cross-section centroid at abscissa x; φ is the cross-section rotation at abscissa x; primes indicate derivation with respect to x. The axis stretching is given by

$$\bar{\lambda} = \sqrt{(1+\bar{u}')^2 + (\bar{w}')^2}. \tag{2}$$

It can be shown [15]—for an elastic material obeying Hooke's law,[1] i.e., $\sigma = E(\lambda-1)$, where λ is the stretching at the point (x,z)—that the normal force and the bending moment can be exactly evaluated as

$$N = EA(\bar{\lambda}-1), \tag{3}$$

$$M = -EI\varphi'. \tag{4}$$

Considering the applied end loads, the normal force and the bending moment can also be written as

$$N = -P\cos\varphi + R\sin\varphi, \tag{5}$$

$$M = M_\ell - R[(\ell+\bar{u}_\ell) - (x+\bar{u})] - P(\bar{w}_\ell - \bar{w})$$
$$= M_0 + R(x+\bar{u}) + P\bar{w}, \tag{6}$$

where, without loss of generality, it was assumed in the last of (6) that $\bar{u}_0 = 0$ and $\bar{w}_0 = 0$. Hence, combining (3) and (5), as well as (4) and (6)

$$EA(\bar{\lambda}-1) = -P\cos\varphi + R\sin\varphi, \tag{7}$$

$$-EI\varphi' = M_\ell - R[(\ell+\bar{u}_\ell) - (x+\bar{u})] - P(\bar{w}_\ell - \bar{w})$$
$$= M_0 + R(x+\bar{u}) + P\bar{w}. \tag{8}$$

After derivation with respect to x and taking (1) into account, (8) is rewritten as

$$-EI\varphi'' = R(1+\bar{u}') + P\bar{w}' = \bar{\lambda}(R\cos\varphi + P\sin\varphi). \tag{9}$$

From (7), the axis stretching is

$$\bar{\lambda} = 1 - \left(\frac{P}{EA}\cos\varphi - \frac{R}{EA}\sin\varphi\right). \tag{10}$$

Finally, (10) in (9) leads to a second-order differential equation for the rotations:

$$EI\varphi'' + \left[1 - \left(\frac{P}{EA}\cos\varphi - \frac{R}{EA}\sin\varphi\right)\right](R\cos\varphi + P\sin\varphi) = 0. \tag{11}$$

The corresponding non-dimensional equation is

$$\frac{\mathrm{d}^2\varphi}{\mathrm{d}\xi^2} + \frac{p}{\eta}[1 - p(\cos\varphi - \alpha\sin\varphi)](\alpha\cos\varphi + \sin\varphi) = 0, \tag{12}$$

$$p = \frac{P}{EA}, \quad \alpha = \frac{R}{P}, \quad \xi = \frac{x}{\ell}, \quad \eta = \frac{I}{A\ell^2}. \tag{13}$$

The exact non-linear Eq. (12) can be approximated up to the order ε^3, where $0 < \varepsilon \ll 1$, by

$$\frac{\mathrm{d}^2\varphi}{\mathrm{d}\xi^2} + \alpha_1\varphi + \varepsilon\alpha_2\varphi^2 + \alpha_3\varphi^3 = \varepsilon\alpha_0, \tag{14}$$

$$\varepsilon\alpha_0 = -\frac{\alpha p(1-p)}{\eta}, \quad \varepsilon\alpha_2 = -\frac{\alpha p(1-4p)}{2\eta},$$
$$\alpha_1 = \frac{p(1-p+\alpha^2 p)}{\eta}, \quad \alpha_3 = -\frac{p(1-4p+4\alpha^2 p)}{6\eta}. \tag{15}$$

Notice that the non-homogeneous term and the coefficient of the quadratic term are scaled in (14) as of the order ε, since α is null or at least small compared to the unity in the five classic Euler buckling cases, which are the main concern of this study.

[1] Filipisch and Rosales [16] consider other statements for Hooke's law, depending on which stress (engineering, second Piola–Kirchhoff, Cauchy) and strain (linear, Green, Almansi, Hencky) definitions are used.

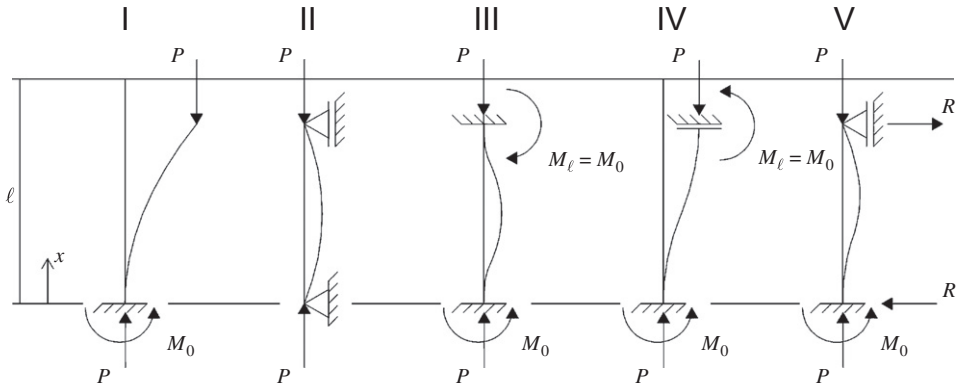

Fig. 2. The five classic Euler buckling cases.

3. Linearised equilibrium equation: classic Euler buckling cases

Fig. 2 refers to the five classic Euler buckling cases [3,4]. To determine the corresponding critical loads for the perfect systems (no load offsets here) it suffices to consider the linearised form of (14):

$$\frac{\mathrm{d}^2\varphi}{\mathrm{d}\xi^2} + \alpha_1\varphi = \varepsilon\alpha_0. \tag{16}$$

Notice that in Cases (I)–(IV) $\alpha=0 \Rightarrow \varepsilon\alpha_0=0$, because no transversal force is needed at the beam ends to secure equilibrium. In Case V, equilibrium requires that

$$\alpha = \frac{R}{P} = \frac{EI\varphi'(0)}{P\ell\left(1+\dfrac{\bar{u}_\ell}{\ell}\right)} \approx \frac{\dfrac{\mathrm{d}\varphi}{\mathrm{d}\xi}(0)}{\dfrac{p(1-p)}{\eta}} \;\Rightarrow\; \frac{\mathrm{d}\varphi}{\mathrm{d}\xi}(0) \approx \frac{\alpha p(1-p)}{\eta}. \tag{17}$$

Yet, from the first of (15) and (17), it is found that for Case V

$$\varepsilon\alpha_0 \approx -\frac{\mathrm{d}\varphi}{\mathrm{d}\xi}(0). \tag{18}$$

In the classical inextensible rod solution, (16) is replaced by

$$\frac{\mathrm{d}^2\varphi}{\mathrm{d}\xi^2} + (k\ell)^2\varphi = \varepsilon\alpha_0, \tag{19}$$

where

$$k\ell = \sqrt{\frac{p}{\eta}} \tag{20}$$

is an approximation for $\sqrt{\alpha_1}$.

Solution to (16)—or equally (19), if $\sqrt{\alpha_1}$ is replaced by $k\ell$—is

$$\varphi = \frac{\varepsilon\alpha_0}{\alpha_1} + C_1\,\sin(\sqrt{\alpha_1}\xi) + C_2\,\cos(\sqrt{\alpha_1}\xi), \tag{21}$$

where C_1 and C_2 are real constants to be determined from the boundary and/or symmetry conditions:

$$\begin{aligned}
&\textit{Case}\ \text{I} \;\Rightarrow\; \varphi(0)=0 \quad\text{and}\quad \frac{\mathrm{d}\varphi}{\mathrm{d}\xi}(1)=0,\\
&\textit{Case}\ \text{II} \;\Rightarrow\; \frac{\mathrm{d}\varphi}{\mathrm{d}\xi}(0)=0 \quad\text{and}\quad \frac{\mathrm{d}\varphi}{\mathrm{d}\xi}(1)=0,\\
&\textit{Case}\ \text{III} \;\Rightarrow\; \varphi(0)=0 \quad\text{and}\quad \varphi\left(\frac{1}{2}\right)=0,\\
&\textit{Case}\ \text{IV} \;\Rightarrow\; \varphi(0)=0 \quad\text{and}\quad \varphi(1)=0,\\
&\textit{Case}\ \text{V} \;\Rightarrow\; \varphi(0)=0 \quad\text{and}\quad \frac{\mathrm{d}\varphi}{\mathrm{d}\xi}(1)=0.
\end{aligned} \tag{22}$$

Critical loads are evaluated from (22), provided the solution (21) is non-trivial. For the inextensible bar, an infinite number of Euler buckling loads p_E are found, the smallest of them being

$$\begin{aligned}
&\textit{Case}\ \text{I} \quad k\ell=\frac{\pi}{2} \;\Rightarrow\; p_E=\frac{\pi^2\eta}{4},\\
&\textit{Case}\ \text{II} \quad k\ell=\pi \;\Rightarrow\; p_E=\pi^2\eta,\\
&\textit{Case}\ \text{III} \quad \frac{k\ell}{2}=\pi \;\Rightarrow\; p_E=4\pi^2\eta,\\
&\textit{Case}\ \text{IV} \quad k\ell=\pi \;\Rightarrow\; p_E=\pi^2\eta,\\
&\textit{Case}\ \text{V} \quad k\ell=4.493 \;\Rightarrow\; p_E=20.19\eta.
\end{aligned} \tag{23}$$

Should the axis stretching be considered, α_1 would play the same role as $(k\ell)^2$. By the way, in Cases I–IV, it is seen that $\alpha_1=p(1-p)/\eta$, since $\alpha=0$. Even in Case V, $\alpha_1=p(1-p)/\eta$ still holds for the unbuckled solution, up to the critical state. Hence, the smallest critical loads considering stretching are

$$\begin{aligned}
&\textit{Case}\ \text{I} \quad \sqrt{\alpha_1}=\frac{\pi}{2} \;\Rightarrow\; p_{cr}=\frac{1-\sqrt{1-\pi^2\eta}}{2},\\
&\textit{Case}\ \text{II} \quad \sqrt{\alpha_1}=\pi \;\Rightarrow\; p_{cr}=\frac{1-\sqrt{1-4\pi^2\eta}}{2},\\
&\textit{Case}\ \text{III} \quad \sqrt{\alpha_1}=2\pi \;\Rightarrow\; p_{cr}=\frac{1-\sqrt{1-16\pi^2\eta}}{2},\\
&\textit{Case}\ \text{IV} \quad \sqrt{\alpha_1}=\pi \;\Rightarrow\; p_{cr}=\frac{1-\sqrt{1-4\pi^2\eta}}{2},\\
&\textit{Case}\ \text{V} \quad \sqrt{\alpha_1}=4.493 \;\Rightarrow\; p_{cr}=\frac{1-\sqrt{1-80.76\eta}}{2}.
\end{aligned} \tag{24}$$

A synthetic relationship between the critical loads, considering axis stretching (p_{cr}) or not (p_E), can be proposed:

$$p_{cr}=\frac{1-\sqrt{1-4p_E}}{2}. \tag{25}$$

Thus, the actual critical load p_{cr} is always larger than the Euler buckling load p_E. Notice that $\eta = I/A\ell^2 = (r/\ell)^2$—where r is the gyration radius of the cross section—is inversely proportional to the square of the slenderness ratio. It is seen that for very slender bars, $p_{cr} \approx p_E$. Yet, as the slenderness ratio decreases, and consequently p_E increases, tending to $\frac{1}{4}$, the critical load tends to twice the Euler buckling load, as it can be seen in Fig. 3.

It is also clear from (25) that there is not such a thing as a critical load p_{cr} when $p_E > \frac{1}{4}$. Taking Case II as an example, it means that there is not a critical load for a bar with $\ell < 2\pi r$, that is to say that the distance between two consecutive inflection points of the *elastica* cannot be smaller than $2\pi r$. Hence, there is a limited number of

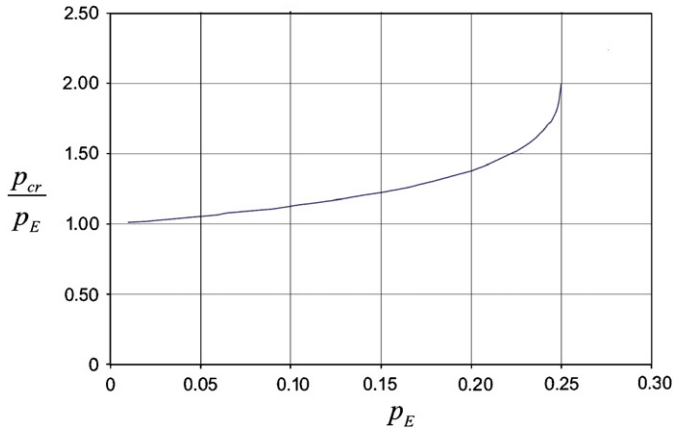

Fig. 3. Critical load for extensible rod as a function of the Euler buckling load.

critical loads, which in Case II happens to be equal to the maximum integer smaller or equal to $(\ell/2\pi r)=(1/2\pi\sqrt{\eta})$. Thus, there will only be five critical loads if $\eta=0.001$ (slenderness ratio equal to 31.6) and 15 critical loads if $\eta=0.0001$ (slenderness ratio equal to 100). Sampaio and Almeida [17] and Magnusson et al. [18] also refer to similar findings.

4. Post-buckling regime: multiple-scales solution

Solution to (14), written as an asymptotic expansion

$$\varphi(\xi)=\varepsilon\varphi_1(\xi_0,\xi_1,\xi_2,\ldots)+\varepsilon^2\varphi_2(\xi_0,\xi_1,\xi_2,\ldots)+\varepsilon^3\varphi_3(\xi_0,\xi_1,\xi_2,\ldots)+\ldots, \tag{26}$$

is investigated via the method of multiple scales, adapting to non-linear statics the technique described in [12] within the context of non-linear dynamics. Instead of time scales, spatial scales will be introduced accordingly:

$$\xi_p=\varepsilon^p\xi,\quad p=0,1,2,\ldots\,. \tag{27}$$

The functions $\varphi_q=\varphi_q(\xi_0,\xi_1,\xi_2,\ldots)$, $q=1,2,\ldots$, will be determined when equations of increasing orders of ε, extracted from (14), are solved and secular terms eliminated (i.e., solvability conditions imposed). The following derivative operators are introduced:

$$\frac{\mathrm{d}}{\mathrm{d}\xi}=D_0+\varepsilon D_1+\varepsilon^2D_2+\varepsilon^3D_3+\ldots,$$

$$\frac{\mathrm{d}^2}{\mathrm{d}\xi^2}=D_0^2+\varepsilon 2D_0D_1+\varepsilon^2(D_1^2+2D_0D_2)+\varepsilon^3(2D_0D_3+2D_1D_2)+\ldots,$$

$$D_p^k=\frac{\partial^k}{\partial\xi_p^k},\quad k=1\text{ or }2,\ \ p=0,1,2,\ldots\,. \tag{28}$$

Taking (26) and (28) in (14) and retaining terms of order ε, leads to

$$D_0^2\varphi_1+\alpha_1\varphi_1=\alpha_0, \tag{29}$$

whose solution, consistently to what has already been seen in (21), is rewritten in the complex form

$$\varphi_1=\frac{\alpha_0}{\alpha_1}+A\exp(\mathrm{i}\sqrt{\alpha_1}\xi_0)+\textit{complex conjugate}, \tag{30}$$

where A is a complex function of $\xi_1,\xi_2,\xi_3,\ldots$.

Terms of order ε^2 in (14) are such that

$$D_0^2\varphi_2+\alpha_1\varphi_2=-2D_0D_1\varphi_1. \tag{31}$$

Notice that the term on the right-hand side of (31) leads to an unbounded solution for φ_2, contrary to what it is expected from the proposed asymptotic expansion (26), according to which any new term added should be a small correction to the accumulated expansion value. Therefore, to enforce that the expansion (26) be uniformly convergent, the right-hand side of (31), which is said to be a secular term, must be eliminated, leading to the so-called solvability condition $D_1\varphi_1=0\Rightarrow A=A(\xi_2,\xi_3,\ldots)$. It is further noticed that the homogeneous solution for φ_2 may be considered as already included in (30) and can thus be disregarded in what follows.

Terms of order ε^3 in (14) lead still to another differential equation

$$D_0^2\varphi_3+\alpha_1\varphi_3=-2D_0D_2\varphi_1-\alpha_2\varphi_1^2-\alpha_3\varphi_1^3, \tag{32}$$

for which the solvability condition (elimination of secular terms) is

$$-2\mathrm{i}\sqrt{\alpha_1}D_2A-2\alpha_2\left(\frac{\alpha_0}{\alpha_1}\right)A-3\alpha_3\left(\frac{\alpha_0}{\alpha_1}\right)^2A-3\alpha_3A^2\bar{A}=0, \tag{33}$$

where $\bar{A}$ is the complex conjugate of A. Solution of (33) will be searched in the form

$$A=\tfrac{1}{2}a\exp(\mathrm{i}\beta),\quad a\in\Re,\ \ \beta\in\Re. \tag{34}$$

It is found that $D_2a=0\Rightarrow a=a(\xi_3,\ldots)$ and

$$\beta=\beta_0+\frac{1}{\sqrt{\alpha_1}}\left\{\alpha_2\left(\frac{\alpha_0}{\alpha_1}\right)+\frac{3\alpha_3}{8}\left[4\left(\frac{\alpha_0}{\alpha_1}\right)^2+a^2\right]\right\}\xi_2. \tag{35}$$

A particular solution of (32) is, therefore,

$$\varphi_3=-\left(\frac{\alpha_2}{\alpha_1}\right)\left[\frac{1}{2}\left(\frac{\alpha_0}{\alpha_1}\right)^2+\frac{1}{4}a^2\right]-\left(\frac{\alpha_3}{\alpha_1}\right)\left(\frac{\alpha_0}{\alpha_1}\right)\left[\frac{1}{2}\left(\frac{\alpha_0}{\alpha_1}\right)^2+\frac{3}{4}a^2\right]+\frac{1}{4}\left[\frac{1}{3}\left(\frac{\alpha_2}{\alpha_1}\right)+\left(\frac{\alpha_3}{\alpha_1}\right)\left(\frac{\alpha_0}{\alpha_1}\right)\right]a^2\exp[2\mathrm{i}(\omega\xi_0+\beta_0)]+\frac{1}{64}\left(\frac{\alpha_3}{\alpha_1}\right)a^3\exp[3\mathrm{i}(\omega\xi_0+\beta_0)]+\textit{complex conjugate}, \tag{36}$$

where

$$\omega=\sqrt{\alpha_1}\left\{1+\left(\frac{\varepsilon\alpha_0}{\alpha_1}\right)\left(\frac{\varepsilon\alpha_2}{\alpha_1}\right)+\frac{3}{8}\left(\frac{\alpha_3}{\alpha_1}\right)\left[4\left(\frac{\varepsilon\alpha_0}{\alpha_1}\right)^2+(\varepsilon a)^2\right]\right\}. \tag{37}$$

Notice that in (36) there is no term in $\exp[\mathrm{i}(\omega\xi_0+\beta_0)]$, since such a term would belong to the homogeneous solution, which is already included in (30).

Finally, from (30), (34) and (36), the post-buckling response up to terms of order ε^3 is

$$\varphi(\xi)=\left(\frac{\varepsilon\alpha_0}{\alpha_1}\right)-\left(\frac{\varepsilon\alpha_2}{\alpha_1}\right)\left[\left(\frac{\varepsilon\alpha_0}{\alpha_1}\right)^2+\frac{1}{2}(\varepsilon a)^2\right]-\left(\frac{\alpha_3}{\alpha_1}\right)\left(\frac{\varepsilon\alpha_0}{\alpha_1}\right)\left[\left(\frac{\varepsilon\alpha_0}{\alpha_1}\right)^2+\frac{3}{2}(\varepsilon a)^2\right]+(\varepsilon a)\cos(\omega\xi+\beta_0)+\frac{1}{2}\left[\frac{1}{3}\left(\frac{\varepsilon\alpha_2}{\alpha_1}\right)+\left(\frac{\alpha_3}{\alpha_1}\right)\left(\frac{\varepsilon\alpha_0}{\alpha_1}\right)\right]\times(\varepsilon a)^2\cos[2(\omega\xi+\beta_0)]+\frac{1}{32}\left(\frac{\alpha_3}{\alpha_1}\right)(\varepsilon a)^3\cos[3(\omega\xi+\beta_0)]. \tag{38}$$

The derivative of φ with respect to ξ will be useful for imposing the boundary conditions:

$$\frac{\mathrm{d}\varphi}{\mathrm{d}\xi}(\xi) = -\omega(\varepsilon a)\,\sin(\omega\xi+\beta_0) - \omega\left[\frac{1}{3}\left(\frac{\varepsilon\alpha_2}{\alpha_1}\right)+\left(\frac{\alpha_3}{\alpha_1}\right)\left(\frac{\varepsilon\alpha_0}{\alpha_1}\right)\right](\varepsilon a)^2\,\sin[2(\omega\xi+\beta_0)] - \frac{3}{32}\omega\left(\frac{\alpha_3}{\alpha_1}\right)(\varepsilon a)^3\,\sin[3(\omega\xi+\beta_0)]. \tag{39}$$

The centroid displacements can be evaluated once $\varphi(\xi)$ and $\mathrm{d}\varphi/\mathrm{d}\xi(\xi)$ are known. For the longitudinal displacement, from the last of (1) and (10), it is found that

$$\frac{\bar{u}}{\ell} = \int_0^{\xi}[(1-p\,\cos\,\varphi+p\alpha\,\sin\,\varphi)\cos\varphi-1]\,\mathrm{d}\xi. \tag{40}$$

Using the power series approximations for $\cos\varphi \approx 1-\varphi^2/2$ and $\sin\varphi \approx \varphi-\varphi^3/6$, (40) is re-written as

$$\frac{\bar{u}}{\ell} = -p\xi+\alpha p\int_0^{\xi}\varphi\,\mathrm{d}\xi-\left(\frac{1-2p}{2}\right)\int_0^{\xi}\varphi^2\,\mathrm{d}\xi-\frac{2}{3}\alpha p\int_0^{\xi}\varphi^3\,\mathrm{d}\xi, \tag{41}$$

which can be evaluated with the help of (38) and the boundary conditions.

For the transversal displacements, from (8), it is found that

$$\frac{\bar{w}}{\ell} = \frac{\bar{w}(1)}{\ell}+\frac{\eta}{p}\left(\left.\frac{\mathrm{d}\varphi}{\mathrm{d}\xi}\right|_1-\frac{\mathrm{d}\varphi}{\mathrm{d}\xi}\right)+\alpha\left[\left(1+\frac{\bar{u}(1)}{\ell}\right)-\left(\xi+\frac{\bar{u}}{\ell}\right)\right] = \frac{\eta}{p}\left(\left.\frac{\mathrm{d}\varphi}{\mathrm{d}\xi}\right|_0-\frac{\mathrm{d}\varphi}{\mathrm{d}\xi}\right)-\alpha\left(\xi+\frac{\bar{u}}{\ell}\right), \tag{42}$$

which can be evaluated with the help of (39) and (41), the boundary conditions and the displacements at either $\xi=1$ or 0. Notice that from (37)

$$\varepsilon a = \sqrt{\frac{8}{3}\left(\frac{\alpha_1}{\alpha_3}\right)\left[\frac{\omega}{\sqrt{\alpha_1}}-1-\left(\frac{\varepsilon\alpha_0}{\alpha_1}\right)\left(\frac{\varepsilon\alpha_2}{\alpha_1}\right)\right]-4\left(\frac{\varepsilon\alpha_0}{\alpha_1}\right)^2}. \tag{43}$$

The determination of the amplitude εa, as in (43), is a key step that can only be achieved once ω has been obtained after the imposition of the boundary conditions. In Case V, there is an additional difficulty, since εa depends on α, which has to be determined iteratively, as it will be seen in Section 9. It is worth mentioning that the multiple-scales solution, in general, and expressions (37)–(43), in particular, are valid for whichever Case I–V is considered, provided the appropriate boundary conditions are used. Each one of these cases will be examined in detail in what follows.

5. Case I: clamped-free beam-column

The boundary conditions (22) for Case I are

$$\varphi(0) = (\varepsilon a)\cos\,\beta_0+\frac{1}{32}\left(\frac{\alpha_3}{\alpha_1}\right)(\varepsilon a)^3\,\cos\,3\beta_0 = 0, \tag{44}$$

$$\frac{\mathrm{d}\varphi}{\mathrm{d}\xi}(1) = -\omega(\varepsilon a)\,\sin(\omega+\beta_0) - \frac{3}{32}\omega\left(\frac{\alpha_3}{\alpha_1}\right)(\varepsilon a)^3\,\sin[3(\omega+\beta_0)] = 0, \tag{45}$$

from which, for the first buckling mode, it is found that $\beta_0=\pi/2$ and $\omega=\pi/2$. The first normalised critical load, from (24), is p_{cr}=0.002474, for $\eta=0.001$. For loads $p>p_{cr}$, displacements can be found from (38), (39), (41)–(43), recalling that $\varepsilon\alpha_0=\varepsilon\alpha_2=0$. Fig. 4 displays post-buckled configurations for distinct values of $p>p_{cr}$.

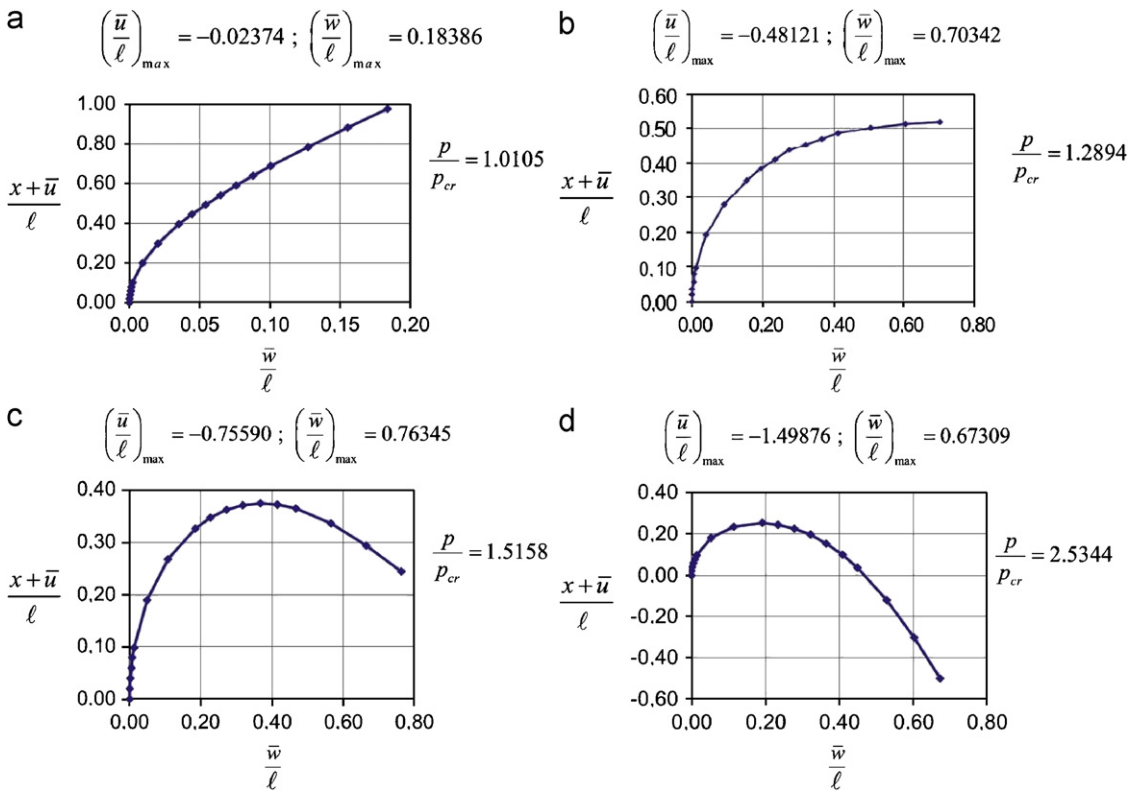

Fig. 4. Post-buckled configurations and maximum displacements for (a) $p/p_{cr}=1.0105$; (b) $p/p_{cr}=1.2894$; (c) $p/p_{cr}=1.5158$; (d) $p/p_{cr}=2.5344$.

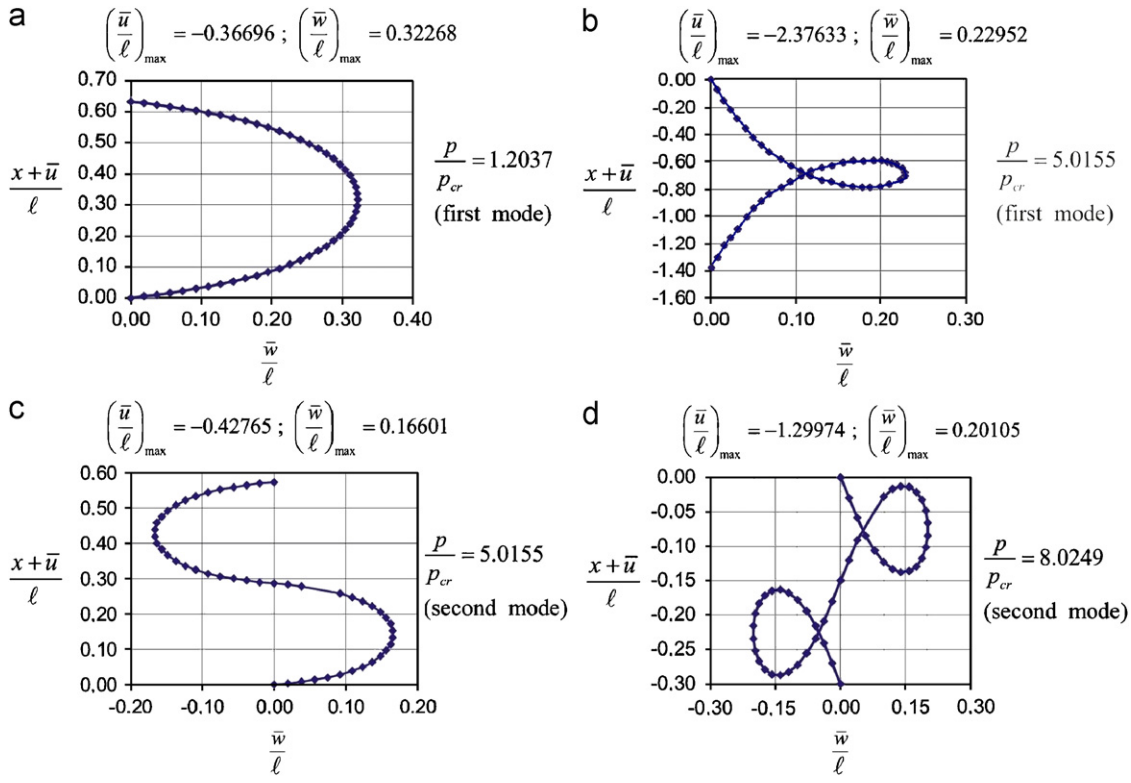

Fig. 5. Post-buckled configurations and maximum displacements for (a) $p/p_{cr} = 1.2037$ (first mode); (b) $p/p_{cr} = 5.0155$ (first mode); (c) $p/p_{cr} = 5.0155$ (second mode); (d) $p/p_{cr} = 8.0249$ (second mode).

6. Case II: hinged–hinged beam-column

The boundary conditions (22) for Case II are

$$\frac{d\varphi}{d\xi}(0) = -\omega(\varepsilon a)\,\sin\,\beta_0 - \frac{3}{32}\omega\left(\frac{\alpha_3}{\alpha_1}\right)(\varepsilon a)^3\,\sin\,3\beta_0 = 0, \tag{46}$$

$$\frac{d\varphi}{d\xi}(1) = -\omega(\varepsilon a)\,\sin(\omega+\beta_0) - \frac{3}{32}\omega\left(\frac{\alpha_3}{\alpha_1}\right)(\varepsilon a)^3\,\sin[3(\omega+\beta_0)] = 0, \tag{47}$$

from which, for the first buckling mode, it is found that $\beta_0 = 0$ and $\omega = \pi$. The first normalised critical load, from (24), is $p_{cr} = 0.009969$, for $\eta = 0.001$. By the way, the number of critical loads is here limited to five. For loads $p > p_{cr}$, displacements can be found from (38), (39), (41)–(43), recalling that $\varepsilon\alpha_0 = \varepsilon\alpha_2 = 0$. Fig. 5 displays post-buckled configurations for distinct values of $p > p_{cr}$.

7. Case III: clamped–clamped beam-column

The boundary and symmetry conditions (22) for Case III are

$$\varphi(0) = (\varepsilon a)\,\cos\,\beta_0 + \frac{1}{32}\left(\frac{\alpha_3}{\alpha_1}\right)(\varepsilon a)^3\,\cos\,3\beta_0 = 0, \tag{48}$$

$$\varphi\left(\frac{1}{2}\right) = (\varepsilon a)\,\cos\left(\frac{\omega}{2}+\beta_0\right) + \frac{1}{32}\left(\frac{\alpha_3}{\alpha_1}\right)(\varepsilon a)^3\,\cos\left[3\left(\frac{\omega}{2}+\beta_0\right)\right] = 0, \tag{49}$$

from which, for the first buckling mode, it is found that $\beta_0 = \pi/2$ and $\omega = 2\pi$. The first normalised critical load, from (24), is $p_{cr} = 0.041174$, for $\eta = 0.001$. For loads $p > p_{cr}$, displacements can be found from (38), (39), (41)–(43), recalling that $\varepsilon\alpha_0 = \varepsilon\alpha_2 = 0$. Fig. 6 displays post-buckled configurations for distinct values of $p > p_{cr}$.

8. Case IV: clamped-guided bar

The boundary conditions (22) for Case IV are

$$\varphi(0) = (\varepsilon a)\,\cos\,\beta_0 + \frac{1}{32}\left(\frac{\alpha_3}{\alpha_1}\right)(\varepsilon a)^3\,\cos\,3\beta_0 = 0, \tag{50}$$

$$\varphi(1) = (\varepsilon a)\,\cos(\omega+\beta_0) + \frac{1}{32}\left(\frac{\alpha_3}{\alpha_1}\right)(\varepsilon a)^3\,\cos[3(\omega+\beta_0)] = 0, \tag{51}$$

from which, for the first buckling mode, it is found that $\beta_0 = \pi/2$ and $\omega = \pi$. The first normalised critical load, from (24), is $p_{cr} = 0.009969$, for $\eta = 0.001$. For loads $p > p_{cr}$, displacements can be found from (38), (39), (41)–(43), recalling that $\varepsilon\alpha_0 = \varepsilon\alpha_2 = 0$. Fig. 7 displays post-buckled configurations for distinct values of $p > p_{cr}$.

9. Case V: clamped–hinged beam-column

The boundary conditions (22) for Case V are

$$\begin{aligned}\varphi(0) = {} & \left(\frac{\varepsilon\alpha_0}{\alpha_1}\right) - \left(\frac{\varepsilon\alpha_2}{\alpha_1}\right)\left[\left(\frac{\varepsilon\alpha_0}{\alpha_1}\right)^2 + \frac{1}{2}(\varepsilon a)^2\right] \\ & - \left(\frac{\alpha_3}{\alpha_1}\right)\left(\frac{\varepsilon\alpha_0}{\alpha_1}\right)\left[\left(\frac{\varepsilon\alpha_0}{\alpha_1}\right)^2 + \frac{3}{2}(\varepsilon a)^2\right] + (\varepsilon a)\,\cos\,\beta_0 \\ & + \frac{1}{2}\left[\frac{1}{3}\left(\frac{\varepsilon\alpha_2}{\alpha_1}\right) + \left(\frac{\alpha_3}{\alpha_1}\right)\left(\frac{\varepsilon\alpha_0}{\alpha_1}\right)\right](\varepsilon a)^2\,\cos\,2\beta_0 \\ & + \frac{1}{32}\left(\frac{\alpha_3}{\alpha_1}\right)(\varepsilon a)^3\,\cos\,3\beta_0 = 0,\end{aligned} \tag{52}$$

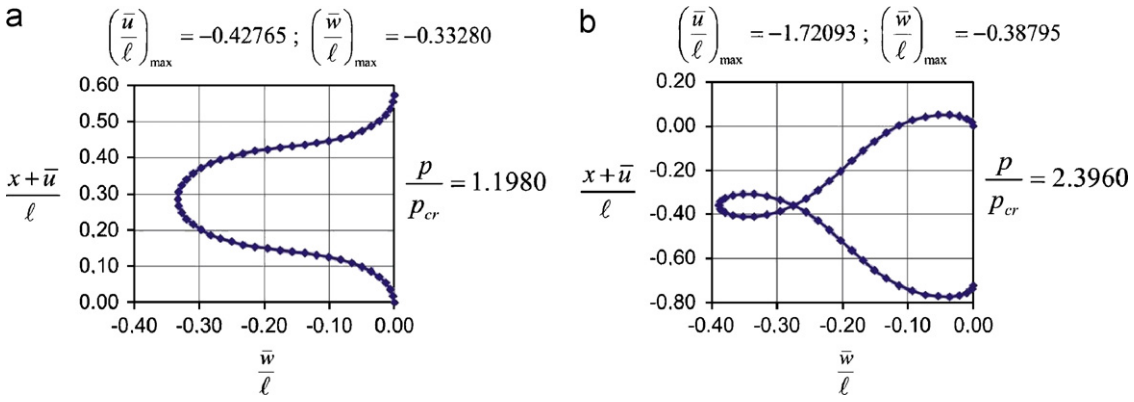

Fig. 6. Post-buckled configurations and maximum displacements for (a) $p/p_{cr} = 1.1980$; (b) $p/p_{cr} = 2.3960$.

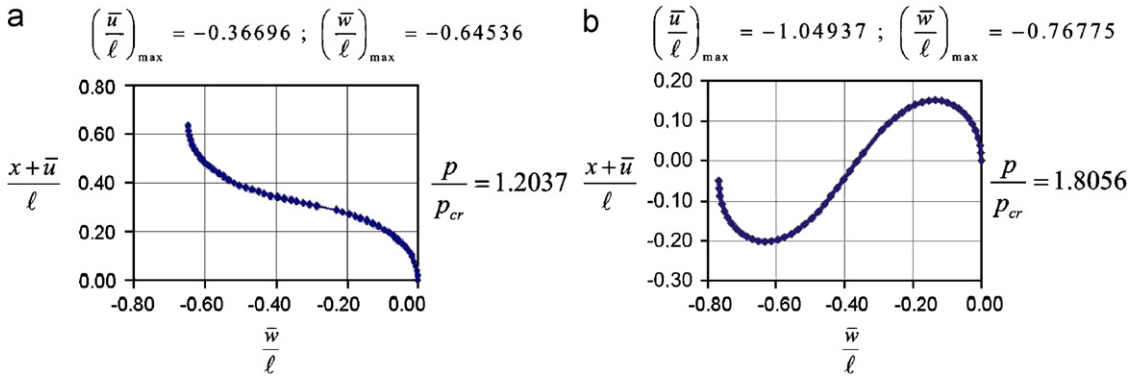

Fig. 7. Post-buckled configurations and maximum displacements for (a) $p/p_{cr} = 1.2037$; (b) $p/p_{cr} = 1.8056$.

$$\frac{d\varphi}{d\xi}(1) = -\omega(\varepsilon a)\sin(\omega+\beta_0) - \omega\left[\frac{1}{3}\left(\frac{\varepsilon\alpha_2}{\alpha_1}\right)+\left(\frac{\alpha_3}{\alpha_1}\right)\left(\frac{\varepsilon\alpha_0}{\alpha_1}\right)\right](\varepsilon a)^2\sin[2(\omega+\beta_0)] - \frac{3}{32}\omega\left(\frac{\alpha_3}{\alpha_1}\right)(\varepsilon a)^3\sin[3(\omega+\beta_0)] = 0, \quad (53)$$

from which, for the first buckling mode, it is found that $\omega+\beta_0=\pi$, β_0 being a solution of (52). The first normalised critical load, from (24), is $p_{cr} = 0.020615$, for $\eta = 0.001$. It should be recalled that here α is non-null in the post-buckling solution, on account of an equilibrium requirement. Notice that for each value of $p > p_{cr}$, an iteration scheme is necessary to evaluate α from (17), $\varepsilon\alpha_0$ and $\varepsilon\alpha_2$ from (15), β_0 from (52), $\omega = \pi - \beta_0$, εa from (43), $\varphi(\xi)$ from (38), $d\varphi/d\xi(\xi)$ from (39), $\bar{u}(\xi)/\ell$ from (41), $\bar{w}(\xi)/\ell$ from (42), α from (17), etc., until convergence has been attained. Fig. 8 displays post-buckled configurations for distinct values of $p > p_{cr}$.

10. Numerical integration

The solution obtained by numerical integration of (12) and (40) is now discussed in this section. For Cases I–IV, since $\alpha = 0$, these equations are uncoupled, which means that we could integrate (12) to obtain $\varphi(\xi)$ and then (40) to obtain $\bar{u}(\xi)/\ell$. Nevertheless, for Case V, since $\alpha = EI\varphi'(0)/P\ell(1+\bar{u}(1)/\ell) \neq 0$, these equations are coupled and must be integrated simultaneously. As for $\bar{w}(\xi)/\ell$, it can be evaluated from (42) in any Case. Since this is not a truly initial-value problem, the fourth-order Runge–Kutta method is not strictly applicable. Yet, it is possible to adapt it in such a way that initial conditions will be imposed for all $\varphi(0)$, $d\varphi/d\xi(0)$ and $\bar{u}(0)/\ell$, even when one of the first two is not strictly a boundary condition, and the integration will proceed for increasing values of ξ. Once $\varphi(1)$, $d\varphi/d\xi(1)$ and $\bar{u}(1)/\ell$ are determined, the boundary conditions at this section can be checked. If they are not satisfied to a certain prescribed small tolerance, an iterative scheme will be required. Note that in Case V, even for the first iteration it is necessary to impose also $\bar{u}(1)/\ell$, to have an initial value for α, both of which values must also converge along the iterative scheme. That is why Case V poses a more complicated convergence pattern. Table 1 displays some results correlating numerical integration and multiple scales results.

Multiple scales results for the maximum transversal displacement, as seen in Table 1, present deviations not larger than 1.5% with respect to the supposedly more accurate results coming out from the numerical integration of the exact Eqs. (12) and (40), for loads 20% larger than the critical one for the corresponding Case I–IV. For Case V, small deviations (2%) were still observed for a load 6.72% larger than the critical one. Deviations are seen to be larger when axial displacements are compared: up to 8.1%, for loads 20% larger than the critical one for the corresponding Case I–IV; and 11.7% for Case V, for a load 6.72% larger than the critical one. For higher loads, comparison was not possible in Case V, since convergence was not achieved in the iterative numerical integration scheme, although the multiple-scales solution was still available.

11. Effect of load offsets

It is well known that Euler buckling is imperfection insensitive, since it corresponds to a stable symmetric bifurcation [6,7]. In other words, small imperfections, such as load offsets, “round off” the

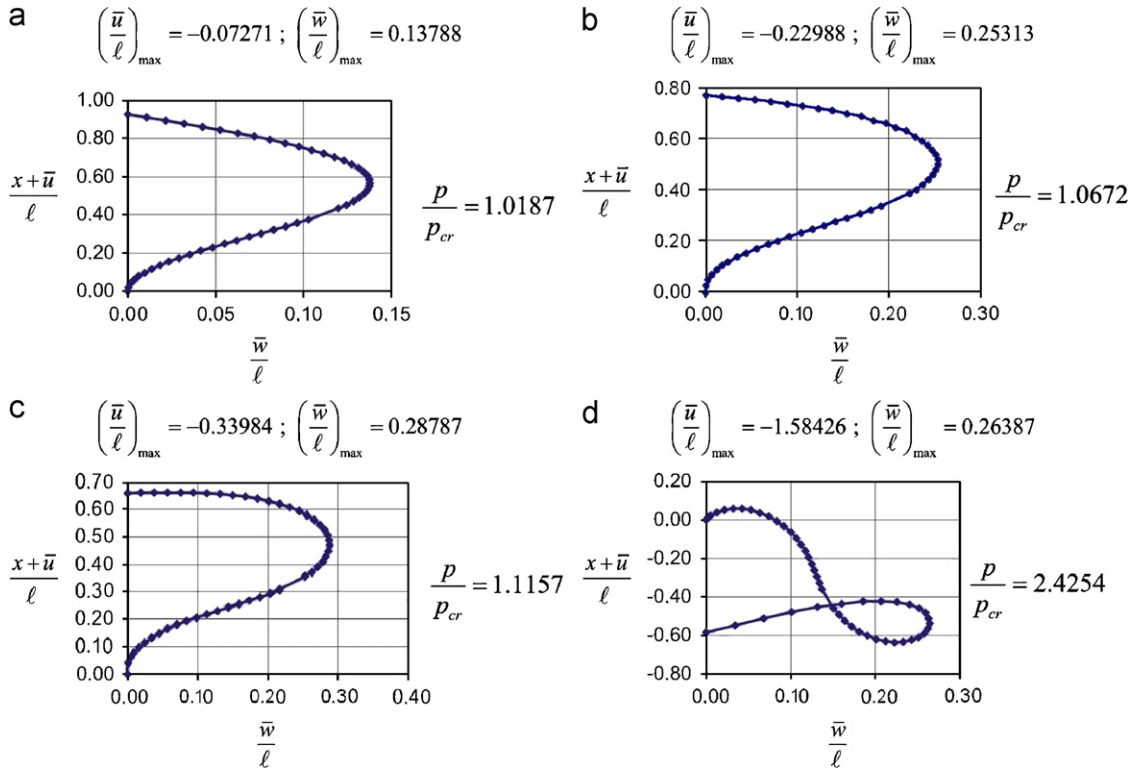

Fig. 8. Post-buckled configurations and maximum displacements for (a) $p/p_{cr} = 1.0187$; (b) $p/p_{cr} = 1.0672$; (c) $p/p_{cr} = 1.1157$; (d) $p/p_{cr} = 2.4254$.

Table 1
Correlation between numerical integration and multiple scales results for $\eta = 0.001$.

Case	I	II	III	IV	V
p/p_{cr}	1.213	1.204	1.214	1.204	1.0672
$A = (\bar{w}/\ell)_{max}$ numerical integration	0.661	0.326	0.331	0.652	0.248
$B = (\bar{w}/\ell)_{max}$ multiple-scales	0.651	0.323	0.333	0.645	0.253
B/A	0.985	0.991	1.006	0.989	1.020
$C = \bar{u}_\ell/\ell$ numerical integration	−0.346	−0.343	−0.396	−0.343	−0.206
$D = \bar{u}_\ell/\ell$ multiple-scales	−0.371	−0.367	−0.428	−0.367	−0.230
D/C	1.072	1.070	1.081	1.070	1.117

equilibrium trajectories close to the bifurcation point and have correspondingly small effects on the post-buckling displacements.

For the sake of an illustration of the formulation generality, a load offset e is here considered for the compressive force P in Cases I and II, as indicated in Fig. 9. As a result of this imperfection, the value of the moment at $x = \ell$ must be equal to

$$M_\ell = Pe = -EI\varphi'(\ell) \Rightarrow \frac{d\varphi}{d\xi}(1) = -\frac{p}{\eta}\left(\frac{e}{\ell}\right). \tag{54}$$

Therefore, for Case I, although (44) remains valid and implies that for the first buckling mode $\beta_0 = \pi/2$, as for the perfect system, the other boundary condition (45) should now be replaced by

$$\frac{d\varphi}{d\xi}(1) = -\omega(\varepsilon a)\sin(\omega+\beta_0) - \frac{3}{32}\omega\left(\frac{\alpha_3}{\alpha_1}\right)(\varepsilon a)^3 \sin[3(\omega+\beta_0)] = -\frac{p}{\eta}\left(\frac{e}{\ell}\right), \tag{55}$$

so that ω is no longer equal to $\pi - \beta_0 = \pi/2$ and must be evaluated from (55) for a given $\mu = e/\ell$.

Fig. 10 displays the post-buckling equilibrium trajectories $(\bar{w}_\ell/\ell)\times p$ for both perfect ($\mu = 0$) and imperfect systems ($\mu = 0.01$) in Case I. As anticipated, minor deviations are noticed.

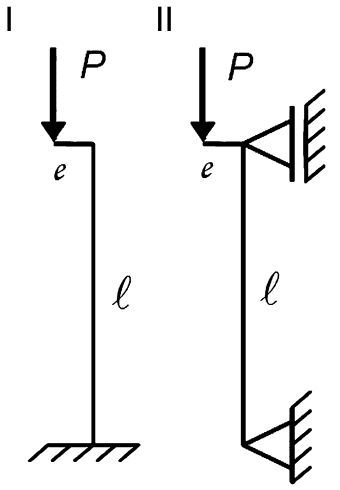

Fig. 9. Load offset in Cases I and II.

For cases in which a transversal reaction could come into play, besides affecting a boundary condition, the load offset would also modify the value of α. For instance, in Case II, the value of α, which was zero for the perfect system, now becomes

$$\alpha = \frac{R}{P} = -\frac{EI\varphi'(\ell)}{P\ell\left(1+\frac{\bar{u}_\ell}{\ell}\right)} = -\frac{\frac{d\varphi}{d\xi}(1)}{\frac{p}{\eta}\left(1+\frac{\bar{u}_\ell}{\ell}\right)} = \frac{\mu}{\left(1+\frac{\bar{u}_\ell}{\ell}\right)}. \tag{56}$$

Since α depends on $\bar{u}_\ell/\ell$, an iterative scheme is necessary to obtain the results. Table 2 displays the ratio between the maximum transversal displacement $(\bar{w}/\ell)_{max}$ for the imperfect system ($\mu = 0.01$) and the corresponding value of the perfect system

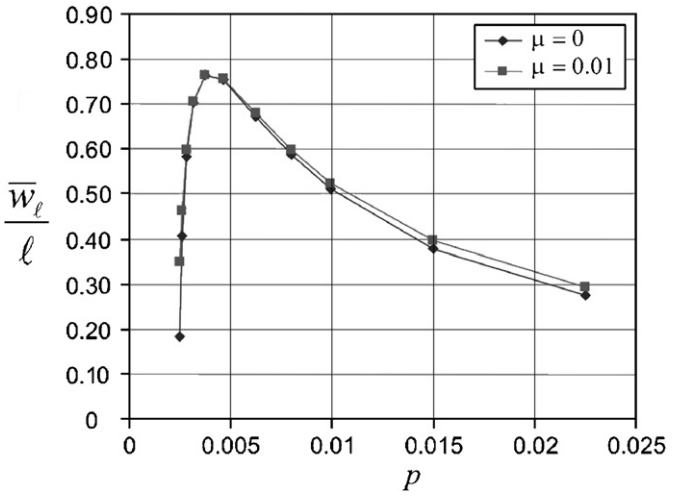

Fig. 10. Post-buckling equilibrium trajectories for the perfect ($\mu = 0$) and imperfect ($\mu = 0.01$) beam-column of Case I.

Table 2
Ratio of the maximum transversal displacement $(\bar{w}/\ell)_{\max}$ for the imperfect system ($\mu = 0.01$) to the corresponding value of the perfect system ($\mu = 0$) in Case II.

p/p_{cr}	$\bar{w}_{\max}(\mu = 0.01)/\bar{w}_{\max}(\mu = 0)$	
	First mode	Second mode
1.2037	1.0083	–
5.0155	1.0341	0.9986
8.0249	–	1.0107

($\mu = 0$) in Case II, for a few values of p/p_{cr}, considering either the first or second buckling modes.

Again, very small deviations are observed, confirming the modest imperfection sensitivity of the post-buckling regime.

12. Conclusions

Very accurate analytical estimates for the post-buckled displacements of slender beam-columns were achieved in this study, well above the critical load, for any one of the classical Euler's cases. The excellence of these results should be attributed to the combination of an efficient perturbation method—though one rarely used in non-linear statics—with an elegant and powerful equilibrium formulation in terms of cross-section rotations—though the one based on transversal displacements is commonplace in the literature. In fact, the multiple scales method, so widely used in non-linear dynamics, proves to be far superior to the classic straightforward procedure (Poincaré's method). It is also remarkable that the results can be shown to be much more accurate for the formulation in terms of rotation, than for the one based on transversal displacements, for the same order of truncation of non-linearities in the equation of motion. It suffices to recall that when this latter has been used in the post-buckling analysis of the pinned–pinned inextensible strut, accurate power-series estimates could only be achieved for loads up to 1.5% above the critical one [3], whereas here, even for the more complex case of an extensible beam-column, the same degree of accuracy was found for loads as high as 20% above the critical value.

Beyond the purely quantitative perspective, the synthesis expressed by the analytical solution (38)–(43), which is valid for whichever boundary condition should be used in each one of the five Euler's Cases, is in itself an achievement, so as to recall that, even in a topic as extensively studied as the buckling and post-buckling analysis of elastic rods, there is still room for new insights.

Acknowledgements

The author acknowledges the support of CNPq under the Grant 304286/2003-6, and is grateful to the precious help received from Paulo Salvador Britto Nigro and Marko Keber in the preparation of figures.

References

[1] L. Euler, Methodus inveniendi lineas curvas maximi minimive proprietate gaudentes, sive solutio problematis isoperimetrici latissimo sensu accepti. Additamentum I. De curvis elasticis, Marcum–Michaelem Bousquet, 1744 (in Latin).
[2] S.P. Timoshenko, History of Strength of Materials, McGraw-Hill, New York, 1953.
[3] S.P. Timoshenko, J.M. Gere, Theory of Elastic Stability, McGraw-Hill Kogakusha, 1961.
[4] J. Ratzersdorfer, Flambagem. I Barras Prismáticas, Instituto de Pesquisas Tecnológicas, Publicação 513, São Paulo, 1954 (a revised version in Portuguese of the book Knickfestigkeit von Stäben und Stabwerken, Springer, Vienna, 1936, in German).
[5] C. Truesdell, The rational mechanics of flexible or elastic bodies, in: L. Euler Opera Omnia (2), vol. 11(2), Füssli, 1960.
[6] W.T. Koiter, On the stability of elastic equilibrium, PhD Thesis, Delft, 1945 (in Dutch; English translation NASA Report TTF-10, 1967).
[7] J.M.T. Tompson, G.W. Hunt, A General Theory of Elastic Stability, Wiley, New York, 1973.
[8] S.S. Antman, The Theory of Rods, Handbuch der Physik, vol. VIa/2, Springer, Berlin, 1972 pp. 641–703.
[9] C.E.N. Mazzilli, Euler buckling and the "elastica" revisited: a unified formulation for the five classical cases, Boletim Técnico do Departamento de Engenharia de Estruturas e Fundações, BT-8710, Escola Politécnica da Universidade de São Paulo, 1987 (in Portuguese).
[10] C.E.N. Mazzilli, Back to the "elastica" and Euler buckling, in: Proceedings of the VIII Ibero–Latin–American Congress of Computational Methods in Engineering, vol. C, Rio de Janeiro, 1987, pp. 201–218 (in Portuguese).
[11] C.Y. Wang, Post-buckling of a clamped-simply supported elastica, International Journal of Non-Linear Mechanics 32 (6) (1997) 1115–1122.
[12] A.H. Nayfeh, D.T. Mook, Nonlinear Oscillations, Wiley, New York, 1979.
[13] J. Fu-ru, Nonlinear analyses for the postbuckling behaviors of annular and circular thin plates, Applied Mathematics and Mechanics 8 (9) (1987) 797–813.
[14] M.K. Wadee, A.P. Bassom, Characterization of limiting homoclinic behaviour in a one-dimensional elastic buckling model, Journal of Mechanics and Physics of Solids 48 (2000) 2297–2313.
[15] P.M. Pimenta, C.E.N. Mazzilli, Minima correctio methodi inveniendi lineas curvas elasticii, Boletim Técnico do Departamento de Engenharia de Estruturas e Fundações, BT-8613, Escola Politécnica da Universidade de São Paulo, 1986 (in Portuguese).
[16] C.P. Filipich, M.B. Rosales, A further study on the postbuckling of extensible elastic rods, International Journal of Non-Linear Mechanics 35 (2000) 997–1022.
[17] R. Sampaio, M.P. Almeida, Buckling of extensible rods, Revista Brasileira de Ciências Mecânicas 7 (1985) 373–385.
[18] A. Magnusson, M. Ristinmaa, C. Ljung, Behaviour of the extensible elastica solution, International Journal of Solids and Structures 38 (2001) 8441–8457.